AGU PUBLICATIONS

JGR

Journal of Geophysical Research: Atmospheres

RESEARCH ARTICLE
10.1002/2016JD025446

Key Points:
- New physics significance of an energy budget method has been shown
- Scale interactions in terms of energy that sustained persistent torrential rainfall events during the Mei-yu season have been shown
- Physical images of upscaled and downscaled energy cascade processes have been shown

Correspondence to:
J. Ling,
Lingjian@lasg.iap.ac.cn

Citation:
Fu, S.-M., J.-H. Sun, J. Ling, H.-J. Wang, and Y.-C. Zhang (2016), Scale interactions in sustaining persistent torrential rainfall events during the Mei-yu season, *J. Geophys. Res. Atmos.*, *121*, 12,856–12,876, doi:10.1002/2016JD025446.

Received 30 MAY 2016
Accepted 15 OCT 2016
Accepted article online 18 OCT 2016
Published online 15 NOV 2016

Scale interactions in sustaining persistent torrential rainfall events during the Mei-yu season

Shen-Ming Fu[1], Jian-Hua Sun[2,3], Jian Ling[4], Hui-Jie Wang[1], and Yuan-Chun Zhang[2]

[1]International Center for Climate and Environment Sciences (ICCES), Institute of Atmospheric Physics, Chinese Academy of Sciences, Beijing, China, [2]Laboratory of Cloud-Precipitation Physics and Severe Storms (LACS), Institute of Atmospheric Physics, Chinese Academy of Sciences, Beijing, China, [3]College of Earth Sciences, University of Chinese Academy of Sciences, Beijing, China, [4]State Key Laboratory of Numerical Modeling for Atmospheric Sciences and Geophysical Fluid Dynamics (LASG), Institute of Atmospheric Physics, Chinese Academy of Sciences, Beijing, China

Abstract Energy budgets based on the temporal scale separation were used to investigate two persistent torrential rainfall events over the Yangtze River Basin during the 2010 Mei-yu season. Interactions between the precipitation-related eddy flows and their background circulations were analyzed quantitatively to show the corresponding physical scenario. During the persistent precipitation, the precipitation-related eddy flows and their background circulations sustained their respective energy through different mechanisms. For background circulations, the baroclinic energy conversion and the energy transport dominated their maintenance. In contrast, for precipitation-related eddy flows, the upper, middle, and lower troposphere showed significantly different energy paths: in the upper troposphere, a remarkable downscaled energy cascade process (ECP) of available potential energy occurred, which favored the maintenance of upper level wind perturbations through the baroclinic energy conversion; in the middle troposphere, the energy transport controlled the evolution of eddy flows; in the lower troposphere, a significant downscaled ECP of kinetic energy maintained its intensity, which directly favored the sustainment of the Mei-yu front and the lower level jet. These downscaled ECPs, which reflected the direct effects of background circulations on the eddy flows, dominated the evolution of precipitation-related eddy flows. In contrast, although upscaled ECPs that indicated the feedback effects of eddy flows on their background circulations were also obvious, they were negligible in the variation of background circulations. The further analysis indicates that whether the background circulations could transfer their energy to the precipitation-related eddy flows was determined by their configurations relative to the eddy flows.

1. Introduction

The Mei-yu season is a unique and important climatic phenomenon in East Asia [*Tao*, 1980; *Oh et al*., 1997; *Ninomiya*, 2000; *Sun and Lee*, 2002; *Ding et al*., 2007; *Sampe and Xie*, 2010], which tends to persist for about 1 month in the early summer. A front stretching from the middle reach of the Yangtze River Basin to the Japanese Islands acts as the most important trigger of torrential rainfall during this period [*Sun and Lee*, 2002; *Zhao et al*., 2004]. This front is called the Mei-yu front in China [*Tao*, 1980; *Zhao et al*., 2004], the Changma front in Korea [*Oh et al*., 1997; *Sun and Lee*, 2002], and the Baiu front in Japan [*Akiyama*, 1984; *Ninomiya*, 2000]. The Mei-yu frontal systems often cause torrential and continuous precipitation events, resulting in huge economic losses and major casualties, such as the torrential rainfall event during mid-July 1998 in the Yangtze River basin [*Bei and Zhao*, 2002], the heavy rainfall event on 23 July 1982 over western Japan [*Nagata and Ogura*, 1991], and the extreme precipitation over Busan on 7 July 2009 [*Jeong et al*., 2016].

Owing to its great importance, for years, tremendous efforts have been made to enhance our understanding of the Mei-yu frontal rainfall events [*Hsu and Sun*, 1994; *Kawamura and Murakami*, 1998; *Yeh et al*., 2002; *Sun et al*., 2010; *Fu et al*., 2011; *Wang et al*., 2012; *Luo and Chen*, 2015]. Among these studies, it is a particularly crucial topic to clarify the relationship between the Mei-yu systems and their large-scale background circulations. *Lau et al*. [1988] suggested that the progression and transition of Mei-yu frontal rainband might result from the phase lock between the 40 and 20 day monsoon modes using the station observational data during 1961–1970. A further study of *Chen and Murakami* [1988] showed that the propagation of intraseasonal global divergent circulation could affect the migration of Mei-yu frontal rainband. *Yang and Li* [2003] analyzed the intraseasonal oscillation (ISO) during the Mei-yu season and described the main upper

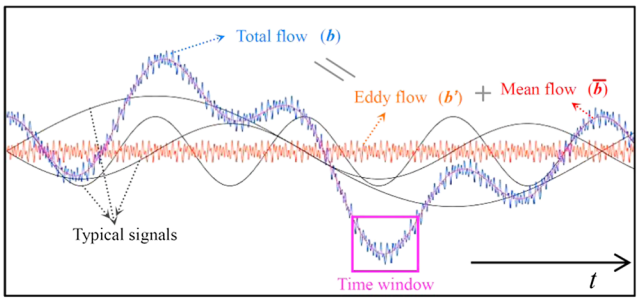

Figure 1. Schematic illustration of the temporal scale separation, where the blue fluctuated curve represents the total flow, the red smoothed curve embedded in the blue fluctuated curve stands for the mean flow (i.e., the background circulation), the orange fluctuated curve is the eddy flow, the three smoothed black curves are the three typical signals in the background circulation, and the purple box is a sample time window.

level ISO pattern for severe flooding as an anticyclonic circulation over the southern Tibetan Plateau. A later study of *Mao and Wu* [2006] showed that the main lower level ISO pattern was conducive to heavy precipitation, which was characterized by an anomalous lower level cyclone over the northern South China Sea. *Liu et al.* [2014] analyzed five continuous extreme rainfall events during the Mei-yu season and proposed that the quasi-biweekly oscillation (QBO) contributed southwesterly anomalies to the Mei-yu frontal convergence, which was favorable for the precipitation. An important role played by the surface cold pool in triggering nocturnal convection ahead of a Mei-yu front has recently been noticed [*Luo and Chen*, 2015]. It should be noted that most previous studies only treated the background circulations (e.g., ISO and QBO) as a favorable background condition that affects the precipitation mainly by enhancing the lower level convergence [*Mao and Wu*, 2006; *Mao et al.*, 2010] and upper level divergence [*Yang and Li*, 2003], by facilitating the moisture transport [*Liu et al.*, 2014], and so on. However, they seldom analyzed how the background circulations fed smaller-scale systems that directly triggered precipitation in the Mei-yu season; nor did they analyze the feedback of these smaller-scale systems to the background circulations. Therefore, the major purpose of this study is to answer the two scientific questions: (a) How do the background circulations feed smaller-scale systems that directly trigger precipitation in the Mei-yu season? (b) What are the features of the feedback of these smaller-scale systems?

This paper is structured as follows: data and methodology are described in section 2. An overview of the selected cases and their fundamental energy characteristics are presented in sections 3 and 4, respectively. Interactions between the precipitation-related eddy flows and their background circulations are discussed in section 5. Finally, the conclusion and discussions are given in section 6.

2. Data and Methods

2.1. Data

Six-hourly climate forecast system reanalysis (CFSR) data (with 0.5° resolution) from the National Centers for Environmental Prediction (NCEP) [*Saha et al.*, 2010] during the 2010 Mei-yu season (from 00 UTC, 3 July to 00 UTC, 17 July 2010) were used for the synoptic analyses and energy calculations. Six-hourly conventional precipitation observation and hourly temperature of black body (TBB) data of the Fengyun-2E satellite (with 0.1° resolution) from the China Meteorological Administration (CMA) were used to investigate the evolution of precipitation and convection activities.

2.2. Energy Budgets

In this study, interactions between the precipitation-related eddy flows and their background circulations are analyzed using the available potential energy (APE) and the kinetic energy (KE). This is because, first, energies are the original driving force for various weather phenomena [*Markowski and Richardson*, 2010], and second, APE and KE are the key factors for the evolution of Mei-yu systems [*Fu et al.*, 2013]. The variation in APE and KE is diagnosed by using a new energy diagnostic scheme (NEDS) proposed by *Murakami* [2011]. This method has been proven effective in evaluating the interaction between weather systems of various scales [*Murakami et al.*, 2011].

By dividing basic meteorological variables into the temporal average and the perturbation component [$b = \overline{b} + b'$ (Figure 1), where b stands for a sample variable, the overbar represents the temporal average, and the prime denotes the perturbation], *Murakami* [2011] derived the NEDS as follows:

Table 1. Abbreviations Used in This Study

Abbreviation	Original Terminology	Abbreviation	Original Terminology
ECP	Energy cascade process	ISO	Intraseasonal oscillation
QBO	Quasi-biweekly oscillation	CFSR	Climate forecast system reanalysis
TBB	Temperature of black body	CMA	China Meteorological Administration
APE	Available potential energy	KE	Kinetic energy
NEDS	New energy diagnostic scheme	KA	Key area
BCEC	Baroclinic energy conversion	REB	Ratio of eddy flows relative to background circulations
K	Total Kinetic energy	A	Total APE
K_M	Kinetic energy of the background circulations	A_M	APE of the background circulations
K_T	Kinetic energy of the eddy flows	A_T	APE of eddy flows
K_I	Interaction kinetic energy	A_I	Interaction APE

$$\partial A_M/\partial t = G(A_M) - C(A_M, K_M) - C(A_M, A_I) - B(A_M) + R(A_M) \quad (1)$$

$$\partial K_M/\partial t = C(A_M, K_M) - C(K_M, K_I) - D(K_M) - B(K_M) \quad (2)$$

$$\partial \overline{A_T}/\partial t = G(\overline{A_T}) - C(\overline{A_T}, \overline{K_T}) - C(\overline{A_T}, A_I) - B(\overline{A_T}) \quad (3)$$

$$\partial \overline{K_T}/\partial t = C(\overline{A_T}, \overline{K_T}) - C(\overline{K_T}, K_I) - D(\overline{K_T}) - B(\overline{K_T}) \quad (4)$$

where $A = \frac{C_p}{2}\left(\frac{p}{p_0}\right)^{2\kappa}\gamma\left(\theta - \langle\overline{\theta}\rangle\right)^2$ is the total APE, $A_M = \frac{C_p}{2}\left(\frac{p}{p_0}\right)^{2\kappa}\gamma\left(\overline{\theta} - \langle\overline{\theta}\rangle\right)^2$ is the APE of background circulations, $A_T = \frac{C_p}{2}\left(\frac{p}{p_0}\right)^{2\kappa}\gamma\theta'^2$ is the APE of eddy flows, and $A_I = C_p\left(\frac{p}{p_0}\right)^{2\kappa}\gamma\theta'\left(\overline{\theta} - \langle\overline{\theta}\rangle\right)$ is defined as the interaction APE [*Murakami*, 2011] (Table 1). In these formulas, C_p is the atmospheric specific heat at constant pressure, p is pressure, p_0 is the reference pressure, κ is the ratio between gas constant and specific heat, γ is static stability index, θ is potential temperature, and $\langle\cdot\rangle$ is the operator of global average. The four types of APE satisfy the relationship of $A = A_M + A_T + A_I$. Similarly, $K = \frac{1}{2}(u^2 + v^2)$ is the total KE, $K_M = \frac{1}{2}\left(\overline{u}^2 + \overline{v}^2\right)$ is the KE of background circulations, $K_T = \frac{1}{2}\left(u'^2 + v'^2\right)$ is the KE of eddy flows, and $K_I = \left(\overline{u}u' + \overline{v}v'\right)$ is defined as the interaction KE (Table 1), where $\mathbf{u} = (u, v, \omega)$ is the three-dimensional (3-D) wind field. The four types of KE also satisfy the relationship of $K = K_M + K_T + K_I$. It should be noted that different from the concept of traditional energy, the interaction energy (i.e., A_I and K_I) that links the energy of background circulations (with a subscript of "M") and the energy of eddy flows (with a subscript of "T") could be negative. The configuration of eddy flows relative to their background circulations determines the effects of interaction energy on the total energy. According to the relationship above, the positive interaction energy enhances the total energy, whereas the negative interaction energy reduces the total energy.

Terms $G(A_M)$ and $G(\overline{A_T})$ denote the diabatic generation/extinction of A_M and A_T, respectively. The scheme reported by *Kuo* [1974] was utilized to evaluate the latent heat release, because it can reasonably capture the main characteristics of the diabatic processes of Mei-yu front [*Zhao et al*., 2004]. The terms in the form of $C(X, Y)$ denote the energy conversion between X and Y; a positive value means that energy is transferred from X to Y, whereas a negative value implies Y is converted into X. $B(A_M)$ and $B(K_M)$ are boundary flux terms of A_M and K_M, respectively. $B(\overline{A_T})$ and $B(\overline{K_T})$ denote boundary flux terms of A_T and K_T, respectively. $R(A_M)$ represents the effects associated with the vertical transport of heat. $D(K_M)$ and $D(\overline{K_T})$ denote the dissipation of K_M and K_T, respectively.

According to *Murakami* [2011], the relationships associated with interaction energies are $C(K_M, K_I) + C(\overline{K_T}, K_I) - F(K_I) = 0$ and $C(A_M, A_I) + C(\overline{A_T}, A_I) - F(A_I) = 0$, where $F(A_I) \approx \mathrm{div}(\overline{A_I\mathbf{u}'})$ and $F(K_I) = \mathrm{div}(\overline{K_I\mathbf{u}'})$ represent the 3-D transport of interaction energies by the eddy flows. div() is the divergence operator. The readers can refer to Appendix A, *Murakami* [2011], and *Murakami et al*. [2011] for more detailed information of NEDS.

2.3. Analyzing Method and Its Physical Significance

The time mean operator in the NEDS method (i.e., the overbar) can be generalized to a running mean operator (i.e., the mean flow $\overline{b}$ also varies with time, but with a larger period than that with the eddy flow b'), which is a low-pass filter. Therefore, through this temporal scale separation, the total flow b is decomposed into the

mean flow $\overline{b}$ (background circulations) and the perturbation b' (eddy flows) (Figure 1). For instance, suppose an "N hour" running mean is performed on the time series b of original data (this time series can be represented by the Fourier series, which include waves of various periods). Then, two distinct combined components are determined: a perturbation component b' that contains the eddy flows with periods no longer than N hours, and a mean component $\overline{b}$ that denotes the combined effects of multiscale systems with periods longer than N hours (i.e., background circulations). Different from the traditional understanding which only focuses on the duration of a target event (e.g., a torrential rainfall event), in this way, we consider a target event in a much larger temporal domain, and this target event can be regarded as occurring within a small fixed time window on the long time series of the background circulations (Figure 1). This is the key point to understand NEDS.

After the decomposition, the perturbation component (i.e., eddy flows) acts as the direct trigger for a heavy rainfall event [*Markowski and Richardson*, 2010], while the mean component (i.e., background circulations) acts as the background condition for the event [*Mao et al*., 2010; *Liu et al*., 2014]. Therefore, equations (1)–(4) can describe how the precipitation-related eddy flows interact with their background circulations. Furthermore, as Figure 1 shows, the background circulations can be decomposed into different dominant weather/climate systems with different time scales, which can be called the typical background circulation signals. These signals are predominant characteristics of the background circulations, and the interactions between eddy flows and their background circulations can be represented considerably by the interactions of eddy flows and the typical background circulation signals. For real cases, the typical signals of background circulations can be determined by using the wavelet analysis [*Erlebacher et al*., 1996]. For example, in this study, we can use the warm season in 2010 (from 1 April 2010 to 30 September 2010) to determine these typical background circulation signals.

Although NEDS is an effective method, it cannot be applied to all types of precipitation events. In fact, energy is mainly determined by the intensity of eddy flows, and it cannot depict the actual pattern of the eddy flow (e.g., convergent or divergent, cyclonic or anticyclonic). For those cases with weak perturbation energy but favorable flow pattern, this method becomes invalid. Furthermore, this method is also not applicable for those short-lived severe precipitation processes (e.g., meso-β-scale rain cluster), during which the hydrostatic approximation is not satisfied (NEDS is based on hydrostatic approximation). On the contrary, those precipitation events which have significant perturbation energy, last a long period, and satisfy the hydrostatic approximation are suitable for using the NEDS analysis.

It is an important issue for the NEDS analysis to determine the length of a time window for calculating the running mean. In fact, there are no unified standards, and different time windows can be used according to different scientific purposes. Because the key scientific question of this study is to show how the scale interactions sustained the persistent torrential rainfall events, we used the significant precipitation period as the length of time window in this study. The significant precipitation period should cover the main life cycle of a rainfall event. That is, it should at least account for 80% of the total accumulated precipitation, and during this period the precipitation-related eddy flows maintain strong intensity and exhibit the evolution trend consistent with the precipitation. Under this condition, equations (1)–(4) can show the dominant factors that sustain the precipitation-related eddy flows.

3. Overview of the Selected Persistent Events

The 2010 Mei-yu season was typical, during which several persistent heavy rainfall events occurred [*Fu et al*., 2013]. The most severe continuous precipitation event occurred on 7–12 July, with a 12 h precipitation gap appearing from 12 UTC, 9 July to 00 UTC, 10 July. During this precipitation gap, the Mei-yu front changed significantly in its intensity and horizontal orientation (Figure 2). Thus, the two 48 h significant precipitation periods, i.e., 12 UTC, 7 July to 12 UTC, 9 July and 00 UTC, 10 July to 00 UTC, 12 July, were treated as two separate cases (referred to as Cases 1 and 2, respectively). In these two precipitation periods, the torrential rainfall triggered severe flash floods, landslides, and urban waterlogging, resulting in substantial casualties and huge economic loss in the Yangtze River Basin. In this study, these two continuous precipitation periods were selected for detailed studies. Correspondingly, the 48 h lifespan, which is common for the persistent precipitation events in Mei-yu seasons [*Tao*, 1980; *Zhao et al*., 2004] was used as the time window for the

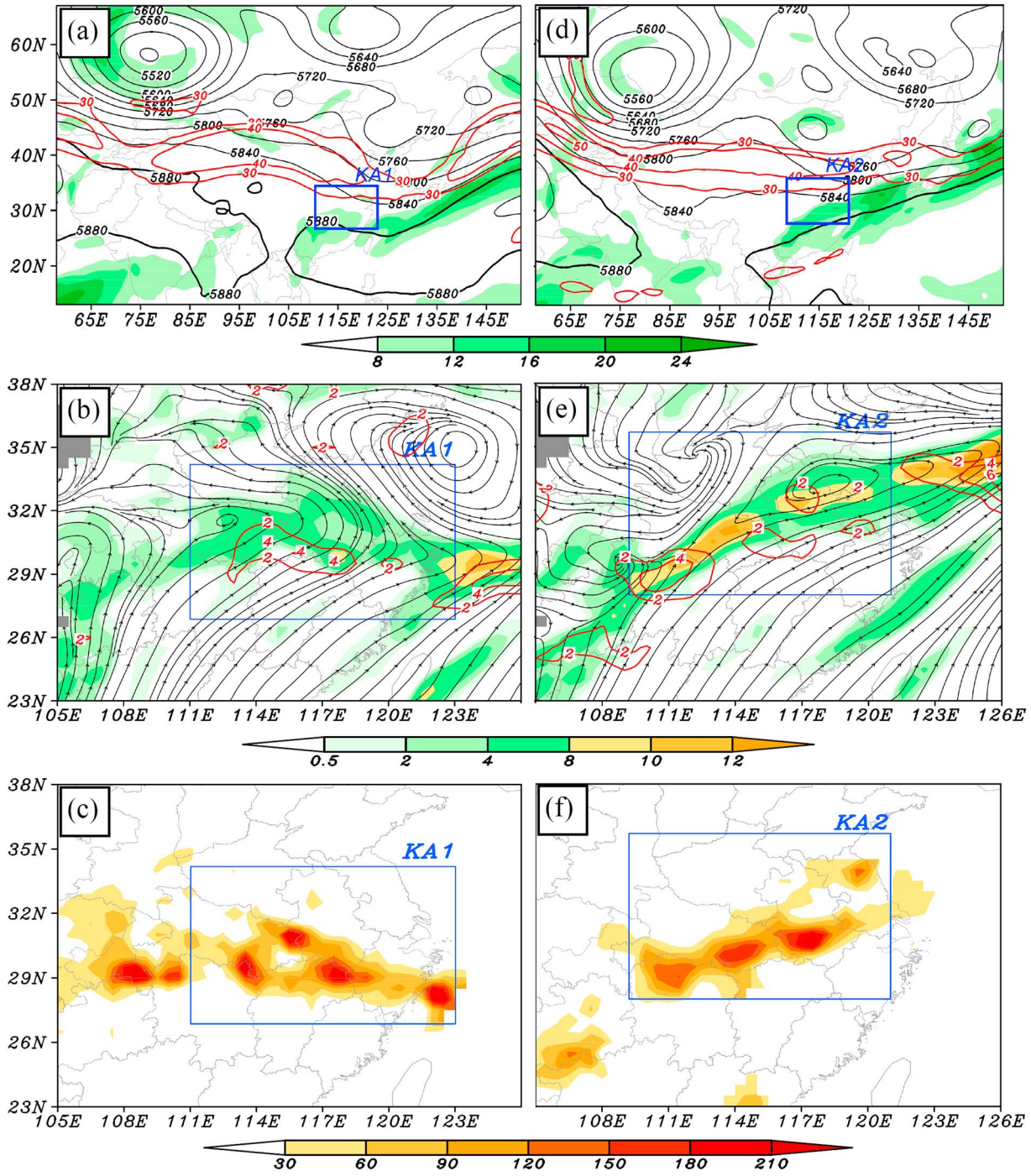

Figure 2. The 48 h averaged geopotential height at 500 hPa (solid, units: geopotential meters (gpm)), averaged lower level jet at 850 hPa (shaded, units: m s^{-1}), and averaged upper level jet at 200 hPa (red dashed line, units: m s^{-1}) during (a) Case 1 and (d) Case 2; the 48 h averaged stream field at 850 hPa during (b) Case 1 and (e) Case 2, where the shading represents the averaged vorticity (units: 10^{-5} s^{-1}) and the red dashed line is the averaged ascent (units: cm s^{-1}); the 48 h accumulated precipitation (shaded, units: mm) during (c) Case 1 and (f) Case 2. The blue rectangles are the KAs of both cases; brown dotted lines are trough lines and shear lines.

NEDS calculation. Moreover, this time window can also satisfy all the conditions for using the NEDS analysis shown in section 2.3.

In order to focus the analysis on the precipitation region, key areas (KAs) were determined according to locations of the Mei-yu front as well as its associated convection activities and precipitation. Therefore, as illustrated in Figure 2, the KA for Case 1 was selected as the area of 27°–34°N, and 111°–123°E (referred

to as KA1), while 27°–34°N and 111°–123°E was used for Case 2 (referred to as KA2). In order to show the overall characteristics of the precipitation-related energy at different layers, the average of budget terms of equations (1)–(4) was first averaged over their respective horizontal domain, and then the vertical integral was calculated. Three layers of equal mass and the total layer were used in the vertical integrals, namely, lower levels from 950 to 700 hPa (950 hPa was used to avoid calculating levels below the terrain), middle levels from 650 to 400 hPa, and upper levels from 350 to 100 hPa, as well as the total layer from 950 to 100 hPa.

3.1. Overview of Weather Systems in the Persistent Events

At 500 hPa, the closed low north of Lake Balkhash, the shortwave trough along the eastern coastline of China, and the subtropical high over the northwestern Pacific Ocean (Figures 2a and 2d), all remained quasi-stationary throughout Cases 1 and 2. This provided relatively stable large-scale conditions that favored the persistence of precipitation. An upper level jet appeared in both cases (Figures 2a and 2d), but the jet was wider in Case 1. Meanwhile, a lower level jet persisted along the northern edge of the western Pacific subtropical high in both cases, but the lower level jet in Case 2 was stronger. Previous studies suggested that the upper level and lower level jets were favorable for Mei-yu frontal precipitation through the ageostrophy-forced secondary circulations [*Markowski and Richardson*, 2010] and the moisture/temperature transport, respectively [*Tao*, 1980; *Zhao et al*., 2004].

A horizontal shear line associated with the Mei-yu front persisted in the lower troposphere throughout Cases 1 and 2 (Figures 2b and 2e). Cyclonic vorticity and active ascending motions were in good match with the shear line. The shear line stretched approximately from west to east in Case 1 (Figure 2b), while the shear line was mainly orientated in a southwest-northeast direction in Case 2 (Figure 2e). The accumulated precipitation of two cases is shown in Figures 2c and 2f, respectively, indicating that convection activities were stronger in Case 1, which was reflected by four heavy rainfall centers with accumulated precipitation above 210 mm (Figure 2c) and a minimum TBB of −92°C in KA1 (not shown). An east-west oriented rain belt was consistent with the lower level shear line (cf. Figures 2b and 2c), implying that the Mei-yu front was the predominant trigger for the precipitation. In Case 2, corresponding to the lower level shear line, the rainband mainly stretched from southwest to northeast (Figure 2f). There were also four precipitation centers but only one of them exceeded 210 mm in KA2. In addition, the minimum TBB was −82°C in Case 2 (not shown). Thus, convection activities in Case 2 were generally weaker than those in Case 1. This can also be confirmed by the ascending motions shown in Figure 3.

In both cases, the intersection of warm and cold air favorable for the production of APE was remarkable (Figure 3). The cold advection was more significant in the upper troposphere, whereas the warm temperature advection was stronger in the middle and lower troposphere. In the middle troposphere, the cold advection associated with the northerly wind was stronger in Case 1 because the shortwave trough along the eastern coastline was stronger in Case 1 (cf. Figures 2a and 2d). In the lower troposphere, notable cold zones appeared in both cases, mainly due to the evaporative cooling [*Bao and Zhang*, 2013; *Luo and Chen*, 2015], which could affect the baroclinic energy conversion (BCEC) of the eddy flows (Appendix A).

4. Basic Energy Features and Main Energy Paths

4.1. Basic Energy Features

Corresponding to the lower level shear line/Mei-yu front, a strong K_T zone with centers above 40 J kg^{-1} remained quasi-stationary throughout Cases 1 and 2 (cf., Figures 2b and 2e and Figures 4a and 4c). Moreover, K_T showed an evolution trend consistent with precipitation over the KAs for both cases (not shown), which means that the first necessary condition for applying the NEDS analysis is satisfied (section 2.3). Moreover, the Mei-yu frontal system has a much larger horizontal scale than its depth. Therefore, according to the criterion defined by *Markowski and Richardson* [2010], which is based on the ratio of the depth of a phenomenon against its horizontal scale, the Mei-yu frontal system satisfies the hydrostatic approximation (this ratio$^2 \ll 1$). This result has also been confirmed by many previous studies [*Tao*, 1980; *Ninomiya*, 2000; *Zhao et al*., 2004]. Therefore, it is suitable to conduct the NEDS analysis on Cases 1 and 2.

Figures 4b and 4d suggest that in both KAs, K_T zones located in the upper and lower troposphere were stronger than that in the middle troposphere. Strong K_T in the upper troposphere was mainly associated with the

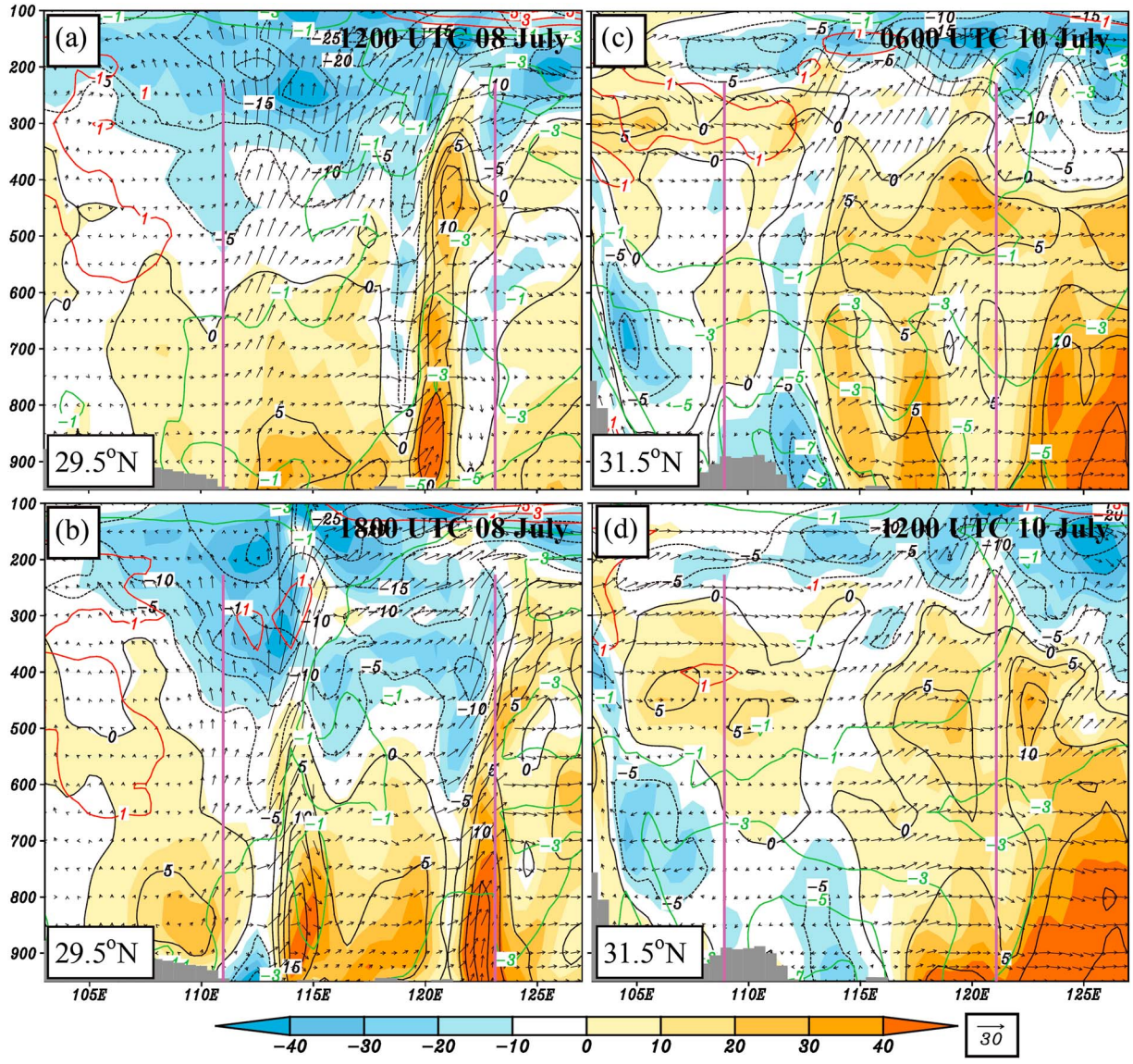

Figure 3. Cross sections along the representative latitudes shown in the bottom left corner of each panel during the maximum precipitation periods in (a, b) Case 1 and (c, d) Case 2. The shading indicates the horizontal advection of temperature (units: 10^{-5} K s^{-1}); black solid and dashed lines are the meridional velocity (units: m s^{-1}); red and green solid lines are the temperature deviations (units: °C); arrows represent the zonal wind and vertical velocity ×100 (units: m s^{-1}); the gray area at the bottom indicates the topography, and the thick purple lines represent the KAs.

upper level perturbation wind (e.g., upper level jet). Those in the lower troposphere were predominantly associated with the Mei-yu front (cf., Figures 2b and 2e and Figures 4a and 4c). In addition, the lower level jet also accounted for a proportion of this significant K_T (cf., Figures 2a and 2d and Figures 4a and 4c).

As Figures 4b and 4d show, for both cases, the APE of eddy flows (A_T), which was predominantly determined by the temperature perturbations (both diabatic/adiabatic processes and temperature advection can result in temperature perturbations), reached its maximum in the lower troposphere, where the evaporative cooling and remarkable temperature advection occurred (Figure 3). The A_T zones in the upper troposphere ranked the second, where the strong cold temperature advection appeared (Figure 3). In contrast, the A_T zones minimized in the middle troposphere, where the adiabatic cooling and the latent heating intensely compensated each other (Figure 3).

From Figure 5, it is clear that K_I and A_I maintained their intensity throughout Cases 1 and 2 (their maximum centers >100 J kg^{-1}), which indicates that heavy precipitation was also closely related to the interaction

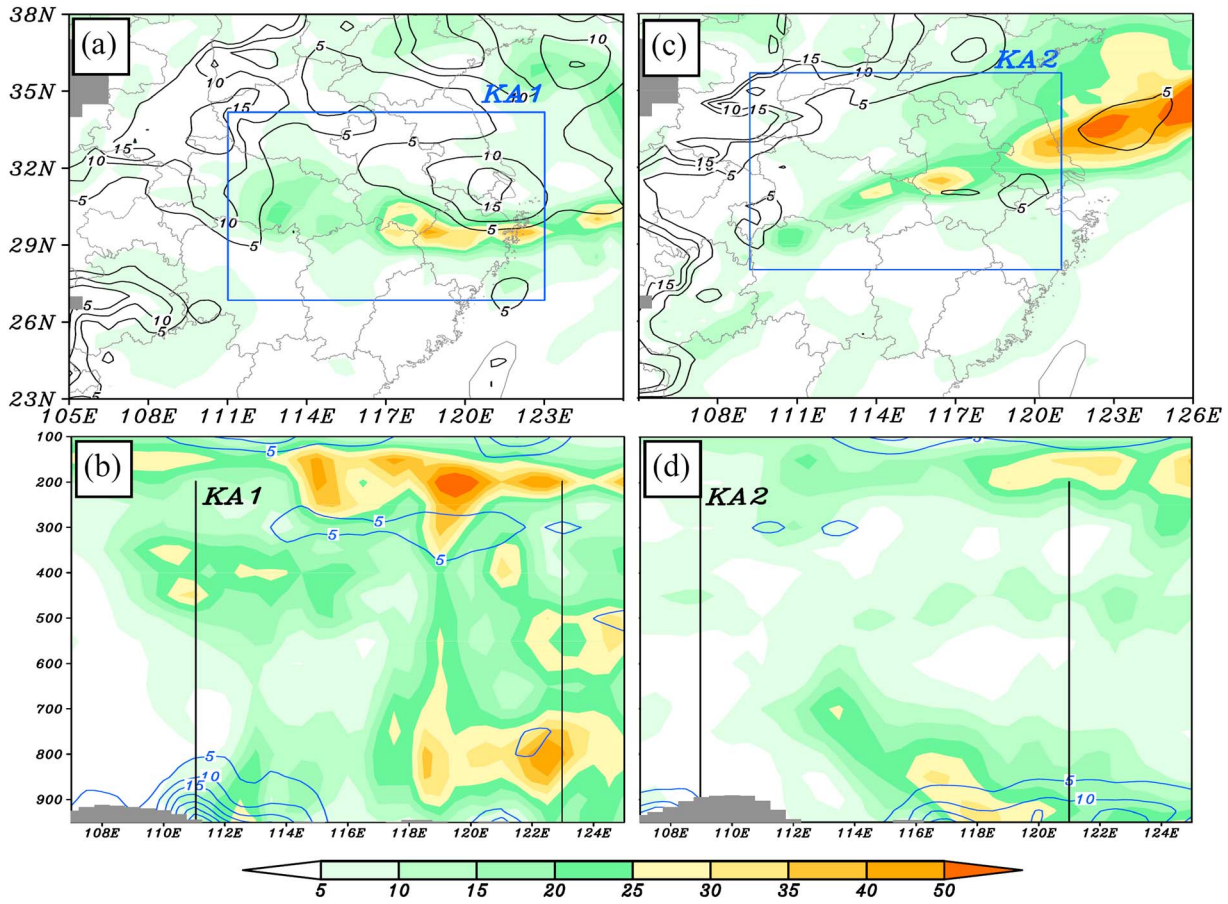

Figure 4. The 48 h averaged K_T (shaded, units: J kg^{-1}) and 48 h averaged A_T (solid contours, units: J kg^{-1}) at 850 hPa during (a) Case 1 and (c) Case 2, where the blue rectangles indicate the KAs. Cross sections of the 48 h averaged K_T (shaded, units: J kg^{-1}) and the 48 h averaged A_T (solid, units: J kg^{-1}) along the representative latitudes as in Figure 3: (b) Case 1; (d) Case 2, where the dark solid lines mark the KAs.

energies. In KAs, K_I and A_I were mainly characterized by stratification, with their maximum zones generally appearing in the upper troposphere. This was because both K_M and A_M maximized at upper levels (Figure 6), where the corresponding perturbation energies were also remarkable (Figures 4b and 4d).

In both KAs, A_M and K_M peaked at upper levels and decreased downward (Figure 6). This was consistent with the basic energy structure of the atmosphere [*Murakami et al.*, 2011]. In order to denote the relative intensity of eddy flows regarding their background circulations, a ratio defined by the energy of eddy flows relative to the corresponding energy of their background circulations (REB) was calculated. As shown in Table 2, the REB of KE maximized at the middle (Case 1) and lower levels (Case 2), whereas at upper levels, REB of KE reached its minimum. Similarly, the REB of APE also reached its maximum at lower levels. Therefore, it can be concluded that strong precipitation-related eddy flows were mainly located in the lower troposphere, whereas the upper troposphere was characterized by more stable background circulations (indicated by smaller REBs). This is consistent with the results of many previous studies [*Tao*, 1980; *Ninomiya*, 2000; *Zhao et al.*, 2004], which show the Mei-yu front was mainly located in the lower troposphere.

4.2. Main Energy Paths

4.2.1. Overall Characteristics

As discussed in section 3.1, the energy budgets were integrated from 950 to 100 hPa to represent the overall characteristics. From Figures 6a and 6b, it is obvious that similar energy paths occurred in both cases:

1. For background circulations, the transport effect $B(A_M)$ dominated the sustainment of A_M. Meanwhile, the diabatic effect $G(A_M)$ and the vertical heat transport effect $R(A_M)$ were also favorable. The APE of

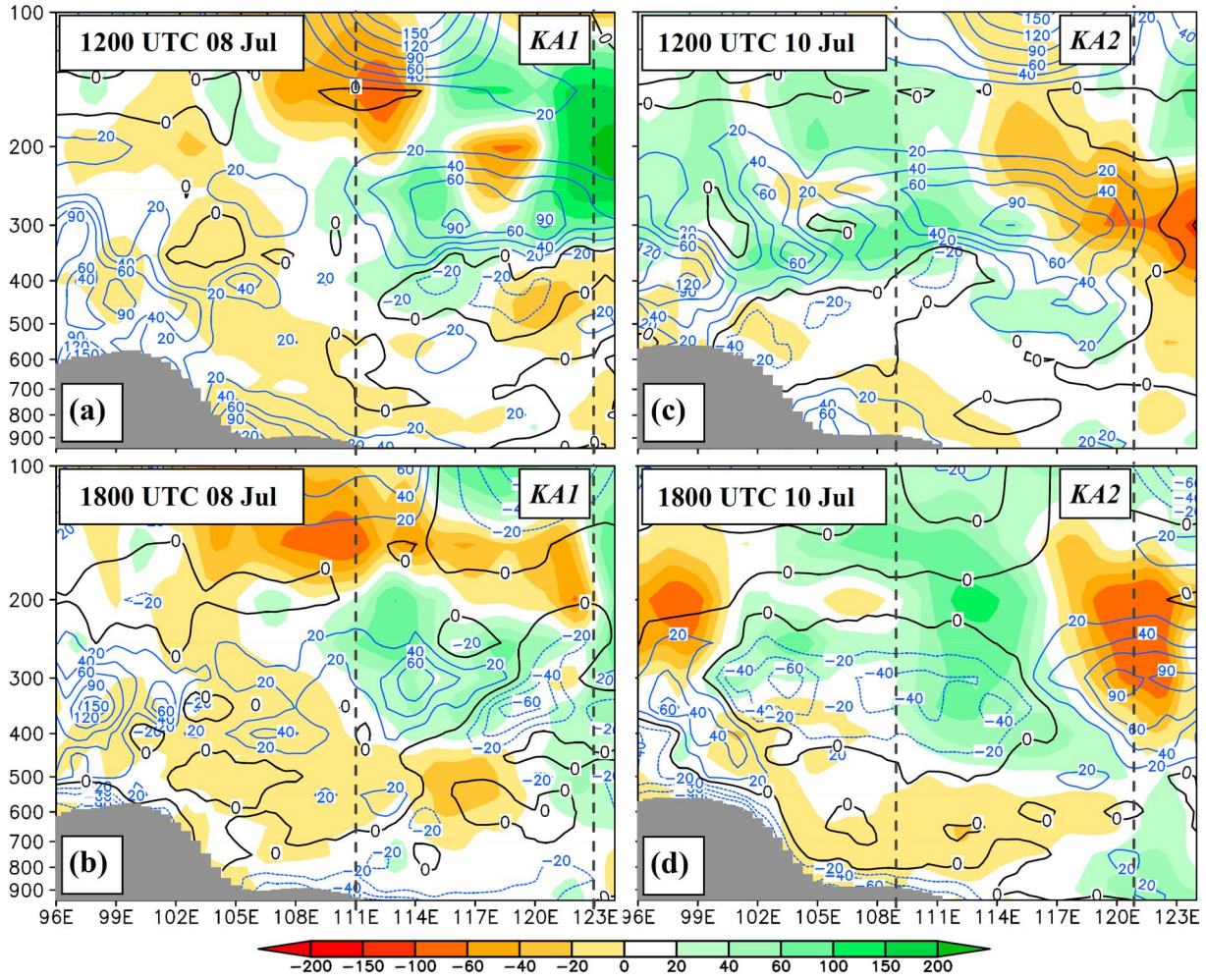

Figure 5. Cross sections of KA meridionally averaged K_I (shaded, units: J kg^{-1}) and A_I (blue dashed and solid contours, with the thick black solid line representing the 0 contour, units: J kg^{-1}) during the maximum precipitation periods in (a, b) Case 1 and (c, d) Case 2.

background circulations (i.e., A_M) served as an energy source, and through the BCEC process, A_M was converted into K_M, which dominated the maintenance of K_M within KAs. In contrast, the transport $B(K_M)$ was the main consumption of K_M.

2. For eddy flows, A_M also acted as the predominant energy source. A small proportion of A_M was transferred to A_T through A_I; i.e., a downscaled energy cascade process (ECP) of APE occurred. During this downscaled ECP, the energy converted from A_M dominated the production of A_I, and the conversion from A_I to A_T dominated the maintenance of A_T. In contrast, the eddy transport $B(\overline{A_T})$ and the BCEC of eddy flows $C(\overline{A_T}, \overline{K_T})$ mainly acted to reduce A_T in KAs. The KE of eddy flows K_T was sustained predominantly through the BCEC, which was closely related to convection activities (Appendix A). A large proportion of K_T was converted into K_I that was transported out of KAs by eddy flows. Moreover, the eddy transport $B(\overline{K_T})$ enhanced K_T in KA1 while dominated the consumption of K_T in KA2.
3. For interaction energies, A_I was mainly produced through its interactions with the background circulations, whereas K_I was generated by its interactions with both the background circulations and the eddy flows. Both KAs served as the interaction energy sources, which exported energy through eddy transports (i.e., $F(A_I) > 0$; $F(K_I) > 0$). The overall energy paths for Cases 1 and 2 are summarized in Figure 7a.

4.2.2. Upper Levels

The energy paths at upper levels (from 350 to 100 hPa) of both cases were very similar to the overall energy paths shown above (cf., Figures 6a, 6b and 6c, 6d), except for terms $R(A_M)$ (Cases 1 and 2), $B(A_M)$ (Case 2), and $F(A_I)$ (Case 1). The vertical heat transport effect $R(A_M)$ was detrimental to the sustainment of A_M at upper levels,

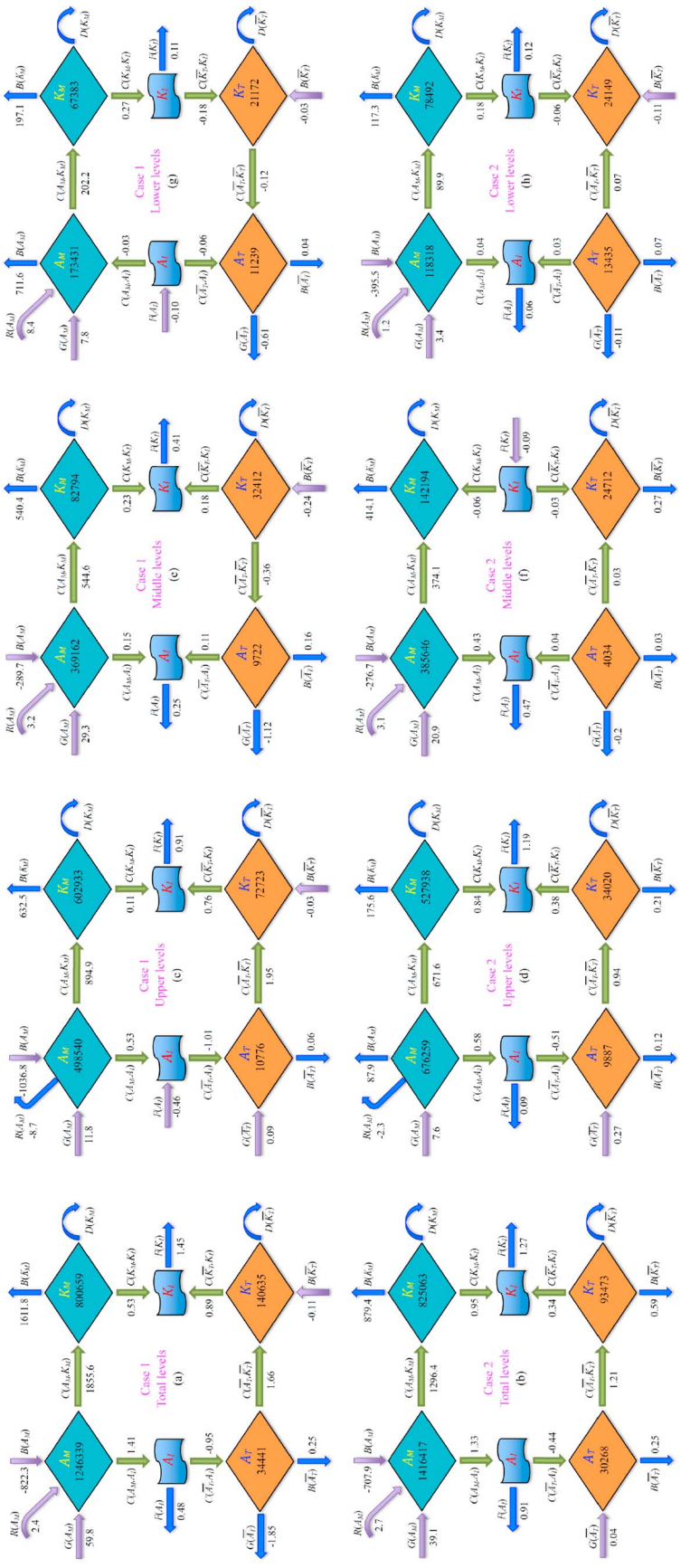

Figure 6. Vertical integral of the KA-averaged energy (units: J m^{-2}) and budget terms of the NEDS (units: W m^{-2}) among the various levels in Case 1 and Case 2. Purple arrows show the effects contributed to the persistence of energy, blue arrows show the opposite, green arrows show the conversion between different types of energy, and the blue curled vector shows the dissipation of KE.

Table 2. The REB of APE and KE at Various Layers in Both Cases

	Case 1		Case 2	
	APE	KE	APE	KE
Upper levels	2.2%	12.1%	1.5%	6.5%
Middle levels	2.7%	39.1%	1.1%	17.4%
Lower levels	6.5%	31.5%	11.3%	30.8%
All levels	2.9%	17.6%	2.1%	11.5%

whereas the situation was opposite at middle and lower levels (Figures 6a–6f). This explains why this term showed different effects at lower levels and total levels. The transport $B(A_M)$ caused net energy divergence in KA2, which reduced A_M, whereas in Case 1 it acted conversely (Figures 6c and 6d). Differences between relative configurations of KAs to their corresponding upper level jets (Figures 2a and 2d) could account for the distinct behaviors of $B(A_M)$ in both cases. Moreover, although downscaled ECPs of APE still dominated the maintenance of A_T at upper levels of both cases, compared to the overall characteristics, KA1 changed to serve as an energy sink for A_I ($F(A_I) < 0$), with eddy flows transporting A_I inward. In summary, energy evolution paths at upper levels of Cases 1 and 2 can be summarized as shown in Figure 7b.

4.2.3. Middle Levels

At middle levels (from 650 to 400 hPa) of both cases, the energy paths associated with background circulations were also similar to the overall energy paths (cf. Figures 6a, 6b and 6e, 6f), whereas the energy paths associated with eddy flows show significant differences. The most important difference is that there is no obvious ECP of APE occurring between the background circulations and eddy flows at middle levels of both cases. This was because A_T was converted to A_I at middle levels (whereas the conversion from A_I to A_T was true at total levels). Other main differences are as follows: (a) Instead of favoring the maintenance of K_T, the BCEC in KA1 converted K_T to A_T. (b) KA2 acted as an energy sink for K_I, with eddy flows transporting energy inward. In summary, energy paths at middle levels of Cases 1 and 2 are shown in Figure 7c.

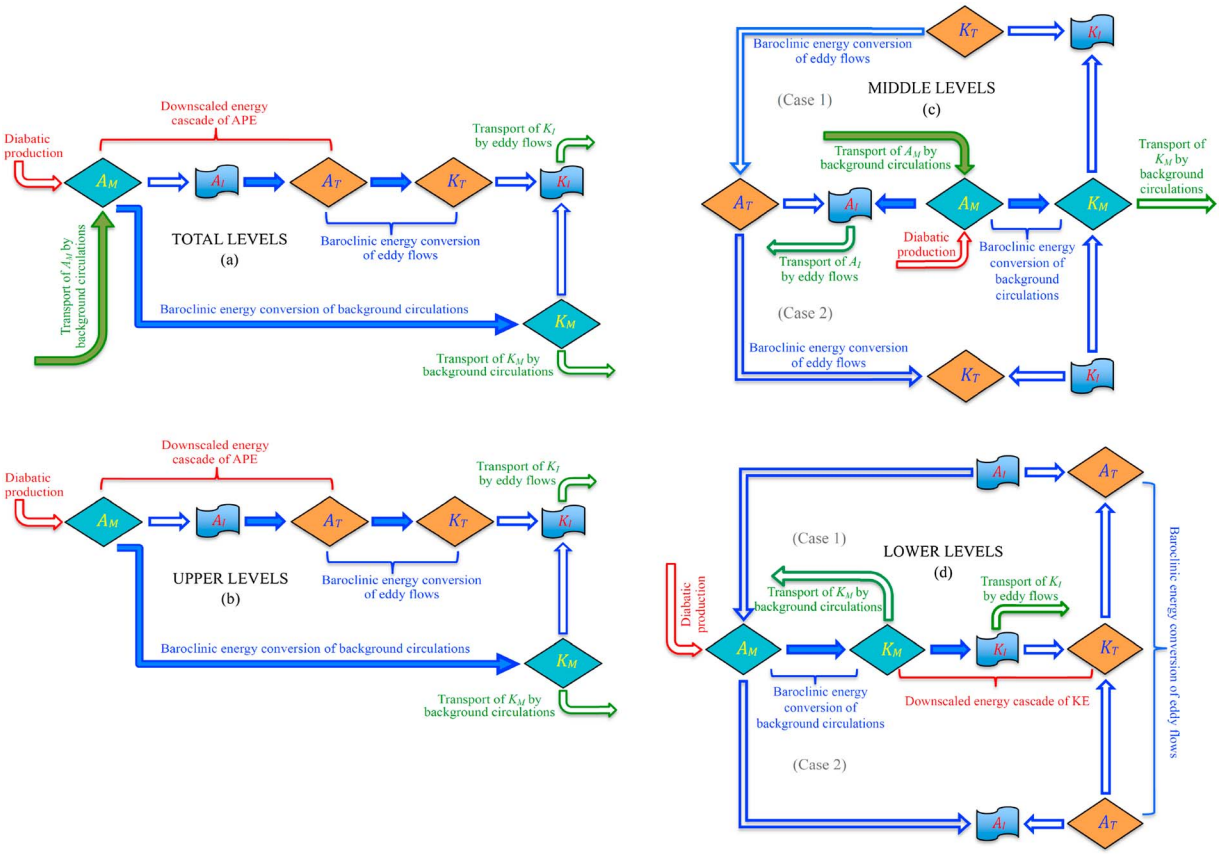

Figure 7. Main energy paths in various layers summarized from both Case 1 and Case 2: (a) total levels; (b) upper levels; (c) middle levels; (d) lower levels. Blue arrows show the energy conversion, green arrows show the transport, and red arrows show the diabatic production of APE. Those factors that dominated the persistence of APE and KE in both Case 1 and Case 2 are shaded.

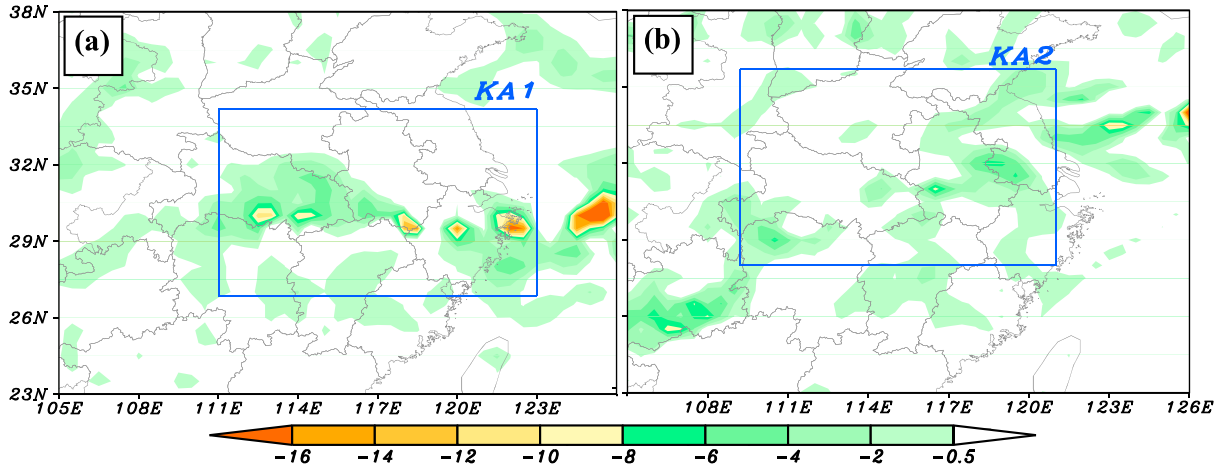

Figure 8. The 48 h averaged term $C(\overline{K_T}, K_I)$ (shaded, units: 10^{-4} J kg^{-1} s^{-1}) at 850 hPa during (a) Case 1 and (b) Case 2, where the blue rectangles indicate the KAs.

4.2.4. Lower Levels

Previous studies [*Tao*, 1980; *Zhao et al.*, 2004] demonstrated that the Mei-yu front was mainly located in the lower troposphere. In this study, Figures 4b and 4d also show that precipitation-related eddy flows were mainly located at lower levels. Therefore, the lower level energy paths that determined the variation of weather systems directly triggering precipitation are analyzed in detail as follows.

In general, the energy paths of background circulations at lower levels were similar in both cases to the overall energy paths (cf., Figures 6a, 6b and 6g, 6h), except for $B(A_M)$ and $C(A_M, A_I)$ in Case 1 (in Case 1, the transport by background circulations reduced A_M, whereas interactions between A_M and A_I slightly favored the maintenance of A_M). In contrast, the energy paths associated with eddy flows showed significant differences at lower levels from those at total levels. The most significant difference is that a remarkable downscaled ECP of KE maintained its intensity at lower levels of both cases (i.e., K_M transferred energy to K_T through K_I), which provided energy for the sustainment of precipitation-related eddy flows directly. As Figures 8a and 8b show, from the spatial perspective, the negative $C(\overline{K_T}, K_I)$ (implying K_I was converted to K_T), which determined the energy income from the downscaled ECP of KE (Appendix B), was generally consistent with the Mei-yu front and the lower level jet in both cases (cf., Figures 8, 2a, 2b, 2d, and 2e). Therefore, the downscaled ECP of KE predominantly acted to sustain the Mei-yu front and the lower level jet, which were known as the crucial triggers for precipitation in the Mei-yu season [*Ninomiya*, 2000; *Zhao et al.*, 2004]. Moreover, as Figures 6g and 6h show, in terms of intensity, the downscaled ECP of KE dominated the maintenance of K_T at lower levels of KA1, and it also was indispensable for the maintenance of K_T in KA2. Another significant difference is that no downscaled ECP of APE appeared at lower levels of both cases. For Case 1, it was because A_I was converted to A_M at lower levels (at total levels, A_M was converted to A_I); for Case 2, it was because A_T was converted to A_I (in total levels, the opposite was true). Other main differences are (a) KA1 served as an energy sink for A_I with eddy flows importing energy inward, and (b) BCEC of eddy flows in Case 1 converted K_T to A_T, which dominated the maintenance of A_T. According to the expression of the term BCEC associated with eddy flows (Appendix A), relative configurations of specific volume and vertical motion in the eddy flows determined the conversion direction of BCEC. The coupling of negative perturbations in the specific volume (associated with the lower level cold temperature perturbations shown in Figure 3a) with ascending motions in Case 1 could account for the conversion from K_T to A_T (lifting of cold air produced APE). In contrast, active warm air is conducive to the release of APE (from A_T to K_T). A summary of the energy paths at lower levels of Cases 1 and 2 is provided in Figure 7d.

Based on the discussions above, during persistent precipitation events, the background circulations and the precipitation-related eddy flows interacted intensely through three main mechanisms: (a) the transport of energies of eddy flows by the background circulations, (b) the transport of interaction energies by the eddy flows, and (c) the ECP. Different from (a) and (b) that reflect the transport effects, the ECP is an energy production process, and the budget analyses shown in Figure 6 have confirmed that the ECPs were crucial in the variation of eddy flows.

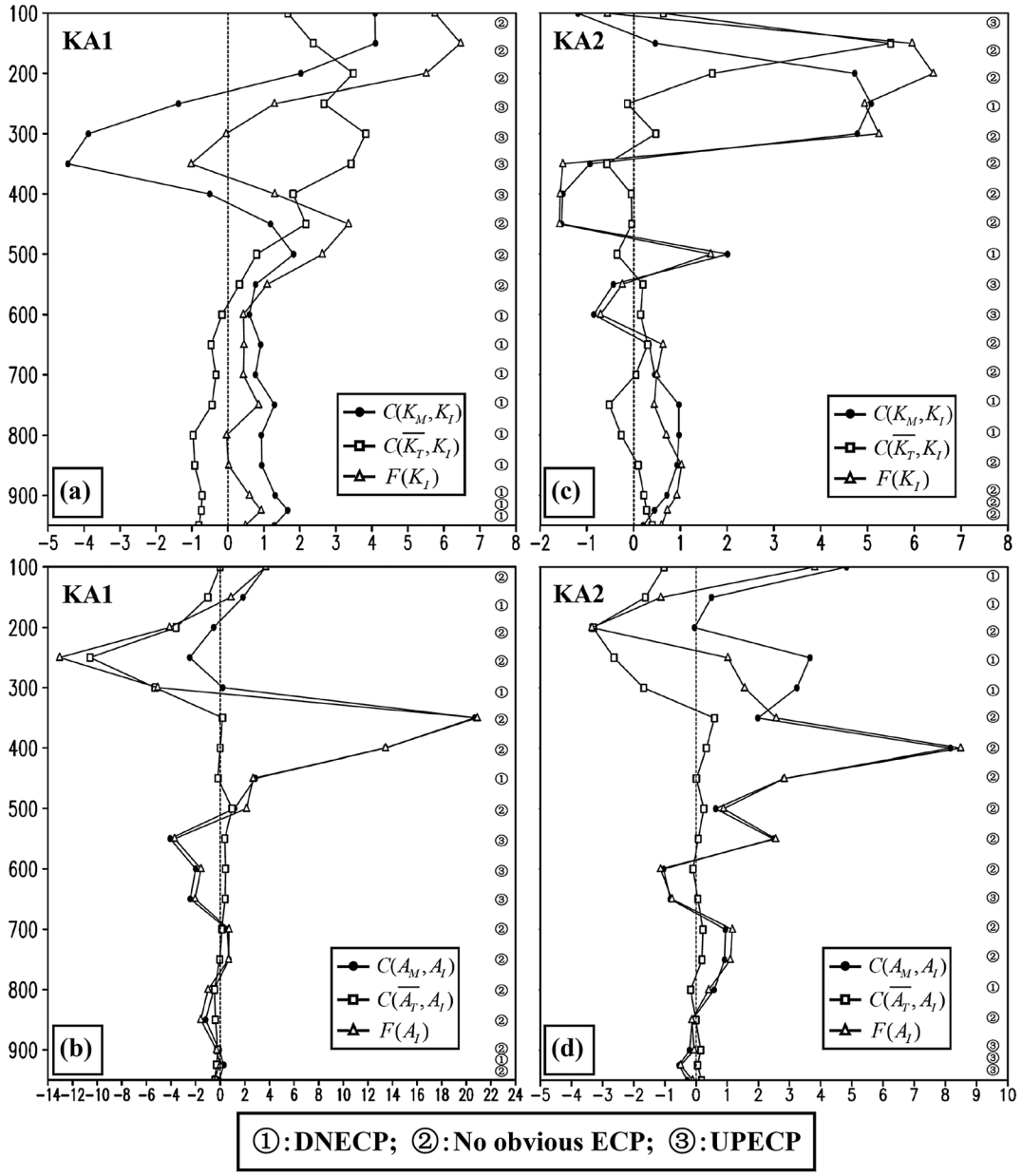

Figure 9. KA-averaged budget terms associated with the interaction energies (units: 10^{-4} J kg^{-1} s^{-1}): (a, b) Case 1; (c, d) Case 2. Numbers on the right-hand side of each panel represent the characteristics of the energy processes, DNECP and UPECP are abbreviations for downscaled and upscaled ECP, respectively.

For the vertical integrated results (Figure 6), only downscaled ECPs were detected. What about the upscaled ECPs that transferred energy from eddy flows to their background circulations? Do upscaled ECPs exist? If so, are they important to the evolution of background circulations? Furthermore, although energies of the background circulations were much stronger than the corresponding energies of eddy flows (Table 2), downscaled ECPs do not always occur. Then, under what conditions can ECPs occur? These questions are addressed in the next section.

5. Energy Cascade Processes

As discussed by *Murakami* [2011], the ECPs cannot occur directly between the eddy flows and their background circulations. Instead, they can only occur through the interaction energies. An ECP includes two

Table 3. The Dominant and Most Detrimental Factors Associated with ECPs of KE[a]

	The UPECP of KE (Dominant Factor/Most Detrimental Factor)			The DNECP of KE (Dominant Factor/Most Detrimental Factor)		
Case 1	Level	$CK_MK_I<0$	$CK_TK_I>0$	Level	$CK_MK_I>0$	$CK_TK_I<0$
	250 hPa	V_h/U_h	U_h/V_v	600 hPa	U_h/V_h	V_h/U_h
	300 hPa	$V_h;V_v/U_h$	$U_h;U_v/V_v$	650 hPa	$U_h;U_v/V_v$	V_h/U_h
	350 hPa	V_v/U_v	U_v/V_h	700 hPa	U_h/V_v	V_h/U_v
	400 hPa	$V_h;V_v/U_v$	$U_h;U_v/V_h$	750 hPa	U_h/V_v	$U_h;V_h/U_v$
	-	-	-	800 hPa	U_h/V_v	$U_h;V_h/U_v$
	-	-	-	850 hPa	$U_h;U_v/V_v$	$U_h;V_h/U_v$
	-	-	-	900 hPa	$U_v/$	V_h/U_v
	-	-	-	925 hPa	$U_v;V_v/$	V_h/U_v
	-	-	-	950 hPa	$V_h;V_v/$	V_h/U_v
Case 2	Level	$CK_MK_I<0$	$CK_TK_I>0$	Level	$CK_MK_I>0$	$CK_TK_I<0$
	100 hPa	V_v/U_v	V_h/U_h	250 hPa	U_h/V_h	U_v/U_h
	550 hPa	V_v/U_h	U_h/V_h	500 hPa	U_v/V_v	V_h/U_h
	600 hPa	V_v/U_h	U_h/V_h	750 hPa	U_h/V_v	$V_h/U_h;U_v$
	-	-	-	800 hPa	$U_h/$	V_h/U_h

[a]"U" represents the zonal factor 1(2) and "V" represents the meridional factor 1(2). The subscript "h" represents the component of the zonal and meridional factors associated with the horizontal eddy transport, and "v" represents the vertical component associated with the vertical eddy transport; "-" means no obvious ECPs.

separate processes, i.e., transitions between the energy of background circulations and the interaction energy, and conversions between the energy of eddy flows and the interaction energy. From equations (2) and (4), $C(K_M, K_I)>0$ represents $K_M => K_I$, and $C\left(\overline{K_T}, K_I\right)<0$ denotes $K_I => K_T$. Therefore, a downscaled ECP of KE occurs: $K_M => K_I => K_T$. When $C(K_M, K_I)<0$ and $C\left(\overline{K_T}, K_I\right)>0$, an upscaled ECP of KE occurs: $K_T => K_I => K_M$. However, if $C(K_M, K_I)$ and $C\left(\overline{K_T}, K_I\right)$ have the same sign, no ECPs occur, and conversions associated with K_I are balanced by the eddy transport $F(K_I)$. Similar to KE, the ECPs of APE occur only when terms $C(A_M, A_I)$ and $C\left(\overline{A_T}, A_I\right)$ have opposite signs. A more detailed discussion of the ECPs and their ideal physical images is given in Appendix B.

5.1. Overview

The directions of ECPs at each level were calculated for both Cases 1 and 2, which were illustrated in Figure 9, from which it can be seen that the downscaled ECPs of KE appeared at 950–600 hPa in Case 1 (Figure 9a) and occurred at 800, 750, 500, and 250 hPa in Case 2 (Figure 9c). The upscaled ECPs of KE appeared at 400–250 hPa in Case 1 and at 600, 550, and 100 hPa in Case 2. The downscaled ECPs of APE occurred at 925, 450, 300, and 150 hPa in Case 1 (Figure 9b), and they appeared at 800, 300, 250, 150, and 100 hPa in Case 2 (Figure 9d). The upscaled ECPs of APE occurred at 650–550 hPa in Case 1 and at 950–900 hPa and 650 hPa in Case 2. As Figures 2 and 3 illustrate, the precipitation-related eddy flows were obviously different in both KAs. Correspondingly, interaction energies in Case 1 differed from those in Case 2 significantly (Figure 5). These differences were the main reasons for the different vertical distributions of ECPs in both cases. In terms of intensity, the downscaled ECPs of both cases were crucial to the evolution of precipitation-related eddy flows, whereas the upscaled ECPs only reacted slightly on the background circulations (Figure 6). This means that a single torrential precipitation event can hardly change its background circulations.

5.2. ECPs of KE

The ideal physical images of ECPs were shown in an easy-to-understand way in Appendix B. However, the ECPs are much more complicated in the real atmosphere, because the eddy flows are characterized by significant unevenness (Figures 2 and 3). In order to determine the dominant factors for different ECPs during a persistent precipitation event, the energy cascade terms were decomposed into several components with obvious physical significance (Appendix B). Correspondingly, the relative importance of these components was compared. For convenience, $\overline{u}\mathrm{div}\overline{u'\mathbf{u}'}$ in $C(K_M, K_I)$ and $\overline{u'\mathbf{u}'}\cdot\mathrm{grad}\overline{u}$ in $C\left(\overline{K_T}, K_I\right)$ were called the zonal factors 1 and 2, respectively. Similarly, $\overline{v}\mathrm{div}\overline{v'\mathbf{u}'}$ in $C(K_M, K_I)$ and $\overline{v'\mathbf{u}'}\cdot\mathrm{grad}\overline{v}$ in $C\left(\overline{K_T}, K_I\right)$ were defined as the meridional factors 1 and 2, respectively. Furthermore, the zonal factors 1 and 2, the

Table 4. Dominant Factors Associated With ECPs of APE[a]

	The Dominant Factor of UPECP of APE			The Dominant Factor of DNECP of APE		
Case 1	Level	$CA_MA_I<0$	$CA_TA_I>0$	Level	$CA_MA_I>0$	$CA_TA_I<0$
	550 hPa	*h*; *v*	*h*	150 hPa	*v*	*v*
	600 hPa	*h*	*h*	300 hPa	*h*	*h*; *v*
	650 hPa	*v*	*h*	450 hPa	*v*	*v*
	-	-	-	925 hPa	*h*	*h*
Case 2	Level	$CA_MA_I<0$	$CA_TA_I>0$	Level	$CA_MA_I>0$	$CA_TA_I<0$
	650 hPa	*v*	*h*	100 hPa	*v*	*h*
	900 hPa	*v*	*v*	150 hPa	*v*	*v*
	925 hPa	*v*	*v*	250 hPa	*h*	*v*
	950 hPa	*v*	*v*	300 hPa	*h*	*h*
	-	-	-	800 hPa	*h*	*v*

[a]The parameter "h" stands for the horizontal component of $C(A_M, A_I)$ and $C(\overline{A_T}, A_I)$ associated with the horizontal eddy transport, and "v" represents the vertical component associated with the vertical eddy transport; "-" means no obvious ECPs.

meridional factors 1 and 2, as well as terms $C(A_M, A_I)$ and $C(\overline{A_T}, A_I)$, were all decomposed into the horizontal and vertical components to compare the relative contribution of the horizontal and vertical transport effects.

Table 3 lists the dominant factors for ECPs of KE. The entire effect of each dominant factor was compared with others based on their total frequency at all energy cascade levels. It should be noted that if two factors were both dominant at the same level, the frequency of each factor was 0.5. From Table 3, it can be seen that the upscaled and downscaled ECPs of KE had different dominant factors. For the upscaled ECPs of KE, U_h was the dominant factor for the conversion from K_T to K_I in both KAs, whereas V_h was the most detrimental factor. In the conversion from K_I to K_M, V_v was the dominant factor, whereas U_h and U_v were the most detrimental factors. For the downscaled ECPs of KE, U_h dominated the conversion from K_M to K_I in both KAs, while V_v was the most detrimental factor. For the conversion from K_I to K_T, V_h was the dominant factor. In contrast, U_v and U_h were the most detrimental factors in Cases 1 and 2, respectively. Moreover, in Case 1, effects associated with the vertical and horizontal eddy transports almost had the same importance. This is because in the upscaled ECPs of KE, $*_h/*_v$ (* stands for *U*/*V*) as shown in Table 3 was 8/8; in the downscaled ECPs, it was 17.5/15.5. However, in Case 2, the horizontal eddy transport was more important ($*_h/*_v$ = 8/4 in the upscaled ECPs and $*_h/*_v$ = 10.5/4.5 in the downscaled ECPs).

5.3. ECPs of APE

As Table 4 shows, regarding the upscaled ECPs of APE, the horizontal component was much more important than the vertical component in Case 1, with $h/v = 4.5/1.5$. In contrast, the vertical component was much more important in Case 2 ($h/v = 1/7$). For the downscaled ECPs of APE, the effects associated with the vertical and horizontal eddy transport almost had the same significance, because the frequency of "*h*" versus that of "*v*" was 3.5/4.5 in Case 1 and 5/5 in Case 2. In general, the ECPs of APE in Case 1 differed remarkably from those in Case 2. As shown in Figures 2 and 3, the Mei-yu front as well as its associated convection activities and precipitation were obviously different in Cases 1 and 2. These differences could explain the differences of ECPs of APE in both cases.

6. Conclusion and Discussion

In this study, two persistent heavy rainfall events during the 2010 Mei-yu season were investigated quantitatively by using the NEDS method to show the basic energy features and energy paths of the Mei-yu systems, as well as the interactions among systems of different scales. Although the Mei-yu front, warm air activities, convection, and rainband show obvious differences in Cases 1 and 2 (Figure 2), which cause obvious differences in the energy paths of these two cases (as Figure 7 shows, these differences are mainly related to the transport effect and BCEC process of the eddy flows), common features of the two cases are still significant, which are characterized by three distinct energy paths over the Mei-yu precipitation region (Figures 7b and 7c):

1. In the upper troposphere, BCEC of the background circulations and the eddy flows both reached maximum. A downscaled ECP of APE maintained its intensity and dominated the sustainment of A_T, while the maintenance of K_T was governed by the BCEC. A_I was mainly generated from its interaction with background circulations, whereas K_I was produced by its interactions with both the background circulations and the eddy flows. The Mei-yu precipitation region served as an energy source of K_I, which might favor ECPs of KE among systems in different regions.
2. In the middle troposphere, no obvious ECPs were detected. A_I was generated from its interactions with both the background circulations and the eddy flows, and the Mei-yu precipitation region was an energy source for A_I.
3. In the lower troposphere, a significant downscaled ECP of KE occurred, which directly favored maintenance of the Mei-yu front and the lower level jet. K_I was predominantly produced by its interaction with the background circulations, and the Mei-yu precipitation region served as an energy source for K_I. Moreover, the Cases 1 and 2 also share common basic energy features: APE and KE of background circulations both peaked in the upper troposphere and decreased downward. The transport by background circulations and the BCEC processes governed the variation of background circulations. The precipitation-related eddy flows were mainly located in the lower troposphere. The transport by eddy flows, the ECPs, and the BCEC processes associated with convection activities dominated the variation of eddy flows.

The background circulations interacted with the precipitation-related eddy flows through three primary mechanisms: the transport of the energy of eddy flows by background circulations, the transport of interaction energies by eddy flows, and the ECPs. The ECPs that are determined by the dynamic (vertical vorticity and horizontal divergence) and thermodynamic features of the background circulations (baroclinicity and stability), and the configuration of eddy flows relative to their background circulations, were crucial to the variation of precipitation-related eddy flows, particularly in the upper and lower troposphere. However, the feedback of eddy flows on their background circulations was negligible to the evolution of background circulations. The ideal physical images of ECPs are presented in Appendix B to facilitate understanding of different types of ECPs.

It is of important scientific value to understand the interactions between the precipitation-related eddy flows and their background circulations. This study has provided an effective method. As discussed in section 2.3, using the NEDS method, we can consider a torrential precipitation event in a much larger temporal domain than its own duration. It means that this precipitation event can be regarded as occurring within a small fixed time window on the long time series of background circulations (Figure 1). By decomposing the background circulations into different typical signals, the interactions between the precipitation-related eddy flows and their background circulations can largely be represented by the interactions of the eddy flows and these typical background circulation signals. Through applying a wavelet analysis to the 2010 warm season (from 1 April 2010 to 30 September 2010), it can be seen that the QBO and ISO signals were the most significant signals in the background circulations during Cases 1 and 2 (not shown). How did these typical background circulation signals interact with the precipitation-related eddy flow? This scientific question will be addressed in future work.

Appendix A

A1. Budget Terms in the NEDS

As shown in *Murakami* [2011], all budget terms of equations (1)–(4) are as follows (definitions of all variables and operators are the same as in the paper):

$G(A_M) = \gamma\left(\overline{T} - \langle\overline{T}\rangle\right)\left(\overline{Q} - \langle\overline{Q}\rangle\right)$ represents the diabatic generation/extinction of A_M.

$C(A_M, K_M) = -\overline{\omega}\,\overline{\alpha}$ stands for the baroclinic energy conversion of the background circulations.

$C(A_M, A_I) = C_p\left(\frac{p}{p_0}\right)^{2\kappa}\gamma\left(\overline{\theta}\text{-}\langle\overline{\theta}\rangle\right)\mathrm{div}\overline{\theta'\mathbf{u}'}$ denotes the conversion between A_M and A_I.

$B(A_M) = C_p\left(\frac{p}{p_0}\right)^{2\kappa}\gamma\mathrm{div}\left[\frac{\left(\overline{\theta}-\langle\overline{\theta}\rangle\right)^2-\langle\overline{\theta}\rangle^2}{2}\overline{\mathbf{u}}\right]$ represents the 3-D transport associated with A_M and other related factors by the background circulations.

$R(A_M) = C_p\left(\frac{p}{p_0}\right)^{2\kappa}\gamma\left(\overline{\theta} - \langle\overline{\theta}\rangle\right)\left(\frac{\partial\langle\overline{\omega}\overline{\theta}\rangle}{\partial p} + \frac{\partial\langle\overline{\omega'\theta'}\rangle}{\partial p}\right)$ denotes the effects associated with the vertical transport of heat by the background circulations and the eddy flows.

$C(K_M, K_I) = \overline{u}\mathrm{div}\overline{u'\mathbf{u}'} + \overline{v}\mathrm{div}\overline{v'\mathbf{u}'} - \frac{\tan\varphi}{a}\left(\overline{u}\overline{u'v'} - \overline{v}\overline{u'u'}\right)$ stands for the conversion between K_M and K_I.

$D(K_M)$ denotes the dissipation of K_M due to friction.

$B(K_M) = \mathrm{div}\left[\left(\frac{\overline{u}^2+\overline{v}^2}{2} + \overline{\Phi}\right)\overline{\mathbf{u}}\right]$ represents the 3-D transport of K_M and mean potential energy by the background circulations.

$G(\overline{A_T}) = \gamma\overline{T'Q'}$ denotes the diabatic generation/extinction of A_T.

$C(\overline{A_T}, \overline{K_T}) = -\overline{\omega'\alpha'}$ stands for the baroclinic energy conversion of the eddy flows.

$C(\overline{A_T}, A_I) = C_p(p/p_0)^{2\kappa}\gamma\overline{\theta'\mathbf{u}'}\cdot\mathrm{grad}\left(\overline{\theta} - \langle\overline{\theta}\rangle\right)$ represents the energy conversion between A_T and A_I.

$B(\overline{A_T}) = C_p\left(\frac{p}{p_0}\right)^{2\kappa}\gamma\mathrm{div}\left[\frac{\overline{\theta'^2}}{2}\overline{\mathbf{u}} + \frac{\overline{\theta'^2\mathbf{u}'}}{2}\right]$ denotes the 3-D transport associated with A_T and other related factors by both the background circulations and the eddy flows.

$C(\overline{K_T}, K_I) = \overline{u'\mathbf{u}'}\cdot\mathrm{grad}\overline{u} + \overline{v'\mathbf{u}'}\cdot\mathrm{grad}\overline{v} + \frac{\tan\varphi}{a}\left(\overline{u}\overline{u'v'} - \overline{v}\overline{u'u'}\right)$ stands for the energy conversion between K_T and K_I.

$D(\overline{K_T})$ denotes the dissipation of K_T due to friction.

$B(\overline{K_T}) = \mathrm{div}\left(\frac{\overline{u'^2}+\overline{v'^2}}{2}\overline{\mathbf{u}}\right) + \mathrm{div}\left[\left(\frac{\overline{u'^2}+\overline{v'^2}}{2} + \Phi'\right)\mathbf{u}'\right]$ stands for the 3-D transport of K_T by the background circulations and the 3-D transport of K_T and perturbation potential energy by the eddy flows.

Appendix B

B1. Ideal Physical Images for ECPs of KE

To illustrate mechanisms and key factors for ECPs in an easy-to-understand way, ideal physics images were created. From *Murakami* [2011], conversions associated with K_I are $C(K_M, K_I) = \overline{u}\mathrm{div}\overline{u'\mathbf{u}'} + \overline{v}\mathrm{div}\overline{v'\mathbf{u}'} - \frac{\tan\varphi}{a}\left(\overline{u}\overline{u'v'} - \overline{v}\overline{u'u'}\right)$ and $C(\overline{K_T}, K_I) = \overline{u'\mathbf{u}'}\cdot\mathrm{grad}\overline{u} + \overline{v'\mathbf{u}'}\cdot\mathrm{grad}\overline{v} + \frac{\tan\varphi}{a}\left(\overline{u}\overline{u'v'} - \overline{v}\overline{u'u'}\right)$, which indicate that if the third term on the right-hand side governs the conversions (e.g., at high latitudes), ECPs always occur. However, in this study, the third term can be neglected because it was much less than the other two terms.

B1.1. Interactions Between K_M and K_I

The first two parts of $C(K_M, K_I)$ are governed by the mean horizontal wind (background circulations) and the divergence of 3-D eddy transport of perturbation momentum. Common configurations are discussed as follows. If $\bar{u} > 0$ (westerly wind), $u' > 0$ (perturbation westerly wind), and convergence occurs, i.e., $\mathrm{div}\overline{u'\mathbf{u}'} < 0$ (this results in $C(K_M, K_I) < 0$), the net effect of 3-D eddy transport is to import perturbation westerly wind into the KA. Therefore, the perturbation westerly momentum increases within the KA. This is equivalent to applying a force within the KA pointing to the east. This force would perform positive work on the mean flow because it is in the same direction as $\bar{u}$. Thus, K_M would be enhanced by the 3-D eddy transport. Supposing an increment of $\Delta u > 0$ to the mean flow due to the transport, relative to the "new" mean state $(\vec{u} + \Delta u)$, new perturbation flow forms due to the adjustment from "old" mean flow to "new" mean flow $[\vec{u} - (\vec{u} + \Delta u) < 0]$. Because the new perturbation flow is in the opposite direction of the new mean state, negative K_I forms and thus K_I decreases within the KA. The decrease of K_I and the increase of K_M correspond to the conversion from K_I to K_M. Other configurations of this term can be explained similarly.

B1.2. Interactions Between K_T and K_I

The first two terms of $C(\overline{K_T}, K_I)$ can be rewritten as $\overline{u'\mathbf{u}'}\cdot\mathrm{grad}\overline{u} = \frac{\overline{u'u'}}{a\cos\varphi}\frac{\partial\overline{u}}{\partial\lambda} + \frac{\overline{u'v'}}{a}\frac{\partial\overline{u}}{\partial\varphi} + \overline{u'\omega'}\frac{\partial\overline{u}}{\partial p}$ and $\overline{v'\mathbf{u}'}\cdot\mathrm{grad}\,\overline{v} = \frac{\overline{v'u'}}{a\cos\varphi}\frac{\partial\overline{v}}{\partial\lambda} + \frac{\overline{v'v'}}{a}\frac{\partial\overline{v}}{\partial\varphi} + \overline{v'\omega'}\frac{\partial\overline{v}}{\partial p}$, implying that Reynolds stress and the horizontal/vertical shear of mean flow (background circulations) are key factors for the interaction. Approximations are made: $\frac{\overline{u'u'}}{a\cos\varphi}\frac{\partial\overline{u}}{\partial\lambda} \approx \overline{u'u'}\frac{\partial\overline{u}}{\partial x'}\frac{\overline{u'v'}}{a}$

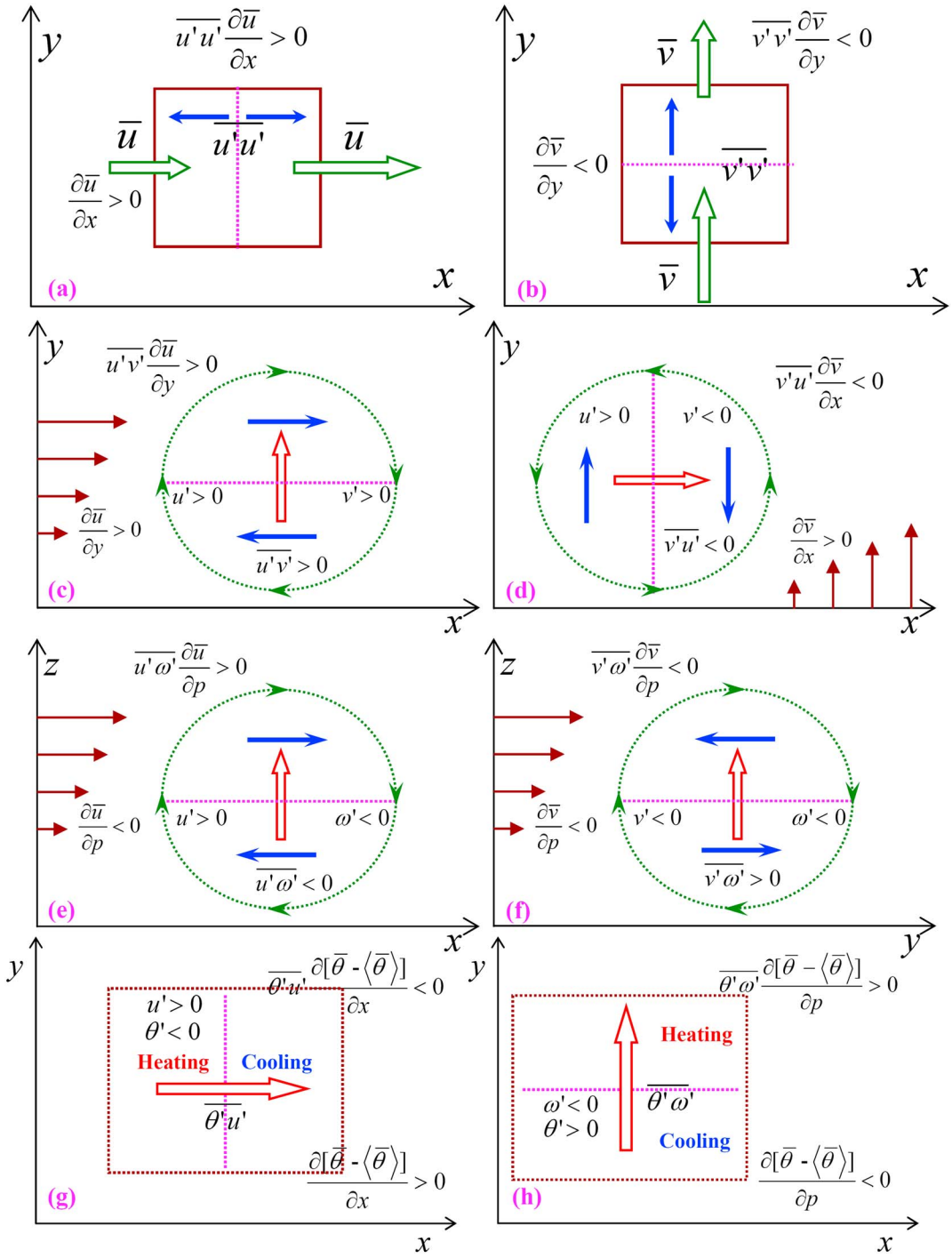

Figure A1. Schematic illustration of the terms $C(\overline{K_T}, K_I)$ and $C(\overline{A_T}, A_I)$, where the dotted purple lines indicate the reference surface, the blue arrows indicate the direction of Reynolds stress, the green open arrows are velocities of the mean flows (background circulations), the red open arrows are the transport directions by the eddy flows, the green cycles represent vortices associated with the mean flow, and the brown vectors represent the horizontal and vertical shear of the mean flow. Illustration of the interactions between K_T and K_I showing the following: (a, b) the situation associated with normal stresses, (c, d) the situation associated with horizontal shear stresses, and (e, f) the situation associated with vertical shear stresses. (g, h) Illustration of the interactions between A_T and A_I.

$\frac{\partial \bar{u}}{\partial \varphi} \approx \overline{u'v'} \frac{\partial \bar{u}}{\partial y}$, $\frac{\overline{v'u'}}{a\cos\varphi} \frac{\partial \bar{v}}{\partial \lambda} \approx \overline{v'u'} \frac{\partial \bar{v}}{\partial x}$, and $\frac{\overline{v'v'}}{a} \frac{\partial \bar{v}}{\partial \varphi} \approx \overline{v'v'} \frac{\partial \bar{v}}{\partial y}$, where terms including $\overline{u'u'}$ and $\overline{v'v'}$ are normal stresses and others are shear stresses. Normal stress is combined with the horizontal divergence of mean flow. Considering a small area with a constant u' (Figure A1) and $\bar{u} > 0$, divergence of the transport of $\overline{u'u'}$ by the mean flow is determined only by the mean flow. If the mean flow diverges zonally, i.e., $\frac{\partial \bar{u}}{\partial x} > 0$, then $\overline{u'u'} \frac{\partial \bar{u}}{\partial x} > 0$ (this results in $C\left(\overline{K_T}, K_I\right) > 0$). Therefore, the mean flow acts to transport $\overline{u'u'}$ (K_T) away from the KA and thus K_T in the KA decreases. Considering a reference surface (the purple dotted line in Figure A1a), the eddy transport of perturbation westerly ($\left(\overline{u'u'}\right)$) is equivalent to applying a force in the same direction as $\bar{u}$ to the right of the surface (as the blue vector shows). To the left of the surface, a force of the same magnitude pointing in the opposite direction of $\bar{u}$ appears. The forces would trigger eddy flow that points in the direction of $\bar{u}$ to the right of the surface and opposite eddy flow to the left of the surface. Because the mean flow is zonally divergent, the net result of the newly triggered K_I in the KA is positive ($\overline{u}_h \cdot u_h' > 0$, where the subscript "$h$" represents the horizontal component). Consequently, K_I is enhanced. The process above illustrates a result of increasing K_I and decreasing K_T, which corresponds to the conversion from K_T to K_I. Another example shown in Figure A1b can be similarly analyzed.

Horizontal shear stresses are shown in Figures A1c and A1d. Because there is $\partial\bar{u}/\partial y > 0$ (mean vertical vorticity), the circulation associated with the mean flow (background circulations) is clockwise as indicated by the green dotted circle in Figure A1c. Term $\overline{u'v'}$ reflects the eddy transport of u' by v'. Supposing positive u' and v' (which results in $C\left(\overline{K_T}, K_I\right) > 0$), then the eddy transport is equivalent to applying a force in the positive x direction to the north of the reference surface and an opposite force to the south of the surface (blue vectors in Figure A1c). Thus, the eddy flow triggered by Reynolds stresses is in the same direction as the mean circulation above and below the reference surface. Therefore, the energy conversion enhances K_I and $C\left(\overline{K_T}, K_I\right) > 0$ also shows that K_I increases due to the conversion from K_T to K_I. The example in Figure A1d can also be explained similarly.

The conversion between K_T and K_I is closely related to baroclinicity of the mean flow (background circulations), which can be reflected by the vertical shear of horizontal wind. Figure A1e displays $\partial\bar{u}/\partial p < 0$, $u' > 0$, and $\omega' < 0$ (which results in $C\left(\overline{K_T}, K_I\right) > 0$); and thus, the transport of u' by ω' is equivalent to applying a force in the positive x direction above the reference surface and an opposite force below the surface (blue vectors in Figure A1e). Because the circulation associated with the mean flow is clockwise, the newly triggered eddy flows occur in the same direction as the mean circulation above and below the surface, which implies an enhancement of K_I owing to the conversion from K_T to K_I. Another example is illustrated in Figure A1f, which can be explained in a similar way.

B2. Ideal Physical Images of ECPs of APE

Terms associated with A_I are $C(A_M, A_I) = C_p(p/p_0)^{2\kappa}\gamma(\overline{\theta}\text{-}\langle\overline{\theta}\rangle)\mathrm{div}\overline{\theta'\mathbf{u}'}$ and $C\left(\overline{A_T}, A_I\right) = C_p(p/p_0)^{2\kappa}\gamma\overline{\theta'\mathbf{u}'}\cdot\mathrm{grad}\left(\overline{\theta}\text{-}\langle\overline{\theta}\rangle\right)$, which are determined by the mean thermodynamic status $\left(\overline{\theta}\text{-}\langle\overline{\theta}\rangle\right)$ and 3-D eddy transport of heat. Because the mean status is stable ($\gamma > 0$) and $C_p(p/p_0)^{2\kappa} > 0$, signs of these two terms are only determined by $\left(\overline{\theta}\text{-}\langle\overline{\theta}\rangle\right)\mathrm{div}\overline{\theta'\mathbf{u}'}$ and $\overline{\theta'\mathbf{u}'}\cdot\mathrm{grad}\left(\overline{\theta}\text{-}\langle\overline{\theta}\rangle\right)$. However, the interactions associated with APE would be enhanced (weakened) as the stability of background circulations increases (decreases).

B2.1. Interactions Between A_M and A_I

For warm regions $\left[\overline{\theta}\text{-}\langle\overline{\theta}\rangle > 0\right]$, if there is net import of perturbation heating ($\theta' > 0$; $\mathrm{div}\mathbf{u}' < 0$) or net export of perturbation cooling ($\theta' < 0$; $\mathrm{div}\mathbf{u}' > 0$), the warm region would be "heated" by the transport ($\mathrm{div}\overline{\theta'\mathbf{u}'} < 0$; this results in $C(A_M, A_I) < 0$). Thus, A_M would intensify because the mean temperature gradients (background circulations) are enhanced by the transport. The "heating" effects of the 3-D eddy transport in warm regions render the "new" mean state warmer than the older one. Consequently, the negative perturbation of θ relative to the new state forms due to the adjustment of mean flow. This negative perturbation in θ is coupled with the mean warm state, which produces negative A_I. The newly produced negative A_I indicates a reduction of A_I in the KA. This increase of A_M and decrease of A_I denotes the conversion from A_I to A_M.

B2.2. Interactions Between A_T and A_I

The horizontal component of $C(\overline{A_T}, A_I)$ is shown in Figure A1g. Supposing $\partial(\overline{\theta}\text{-}\langle\overline{\theta}\rangle)/\partial x > 0$, $u' > 0$, and $\theta' < 0$ (which results in $C(\overline{A_T}, A_I) < 0$), the transport of θ' by u' is equivalent to heating the left of the reference surface and cooling the right. Because $A_I = C_p(p/p_0)^{2\kappa}\gamma\theta'(\overline{\theta}\text{-}\langle\overline{\theta}\rangle)$ and $\overline{\theta}\text{-}\langle\overline{\theta}\rangle$ increases to the east, the eddy transport results in net negative A_I in the KA, which means that A_I decreases. From equation (3), $C(\overline{A_T}, A_I) < 0$ also indicates the decrease of A_I through the conversion from A_I to A_T.

The vertical eddy transport component of $C(\overline{A_T}, A_I)$ is shown in Figure A1h. Supposing $\partial(\overline{\theta}\text{-}\langle\overline{\theta}\rangle)/\partial p < 0$ (stable flow), $\omega' < 0$, and $\theta' > 0$ (which results in $C(\overline{A_T}, A_I) > 0$), the transport of θ' by ω' is equivalent to heating above the reference surface and cooling below. The transport results in net positive A_I in the KA, and thus A_I enhances. From equation (3), $C(\overline{A_T}, A_I) > 0$ also denotes that A_I increases through the conversion from A_T to A_I.

Acknowledgments
The authors thank the NCEP (http://rda.ucar.edu/datasets) and China Meteorological Administration (http://cdc.cma.gov.cn) for providing the data. Sincere thanks are extended to Da-Lin Zhang, Hong-Bo Liu, and two anonymous reviewers. This research was supported by the National Key Basic Research and Development Project of China (2012CB417201) and the National Natural Science Foundation of China (41375053 and 41505038).

References

Akiyama, T. (1984), A medium-scale cloud cluster in a Baiu front, Part I: Evolution process and fine structure, *J. Meteor. Soc. Jpn*, *62*, 485–504.
Bao, X., and F. Zhang (2013), Impacts of the mountain-plains solenoid and cold pool dynamics, *Atmos. Chem. Phys.*, *13*, 1–18.
Bei, N. F., and S. X. Zhao (2002), Mesoscale analysis of severe local heavy rainfall during the second stage of the 1998 Mei-Yu season, *Chinese J. Atmos. Sci.*, *26*, 526–540.
Chen, T. C., and M. Murakami (1988), The 30–50 day variation of convective activity over the western Pacific Ocean with emphasis on the northwestern region, *Mon. Weather Rev.*, *116*, 892–906.
Ding, Y. H., J. Liu, Y. Sun, Y. J. Liu, J. H. He, and Y. F. Song (2007), A study of the synoptic-climatology of the meiyu system in East Asia, *Chinese J. Atmos. Sci.*, *31*, 1082–1101.
Erlebacher, G., M. Y. Hussaini, and L. Jameson (1996), *Wavelets: Theory and Applications*, 528 pp., Oxford Univ. Press, New York.
Fu, S. M., J. H. Sun, S. X. Zhao, W. L. Li, and B. Li (2011), A study of the impacts of the eastward propagation of convective cloud systems over the Tibetan Plateau on the rainfall of the Yangtze Huai River basin, *Acta Meteorol. Sin.*, *69*, 581–600.
Fu, S. M., F. Yu, D. H. Wang, and R. D. Xia (2013), A comparison of two kinds of eastward-moving mesoscale vortices during the mei-yu period of 2010, *Sci. China Earth Sci.*, *56*, 282–300.
Hsu, W. R., and W. Y. Sun (1994), A numerical study of a low-level jet and its accompanying secondary circulation in a mei-yu system, *Mon. Weather Rev.*, *122*, 324–340.
Jeong, J., D. Lee, and C. Wang (2016), Impact of cold pool on mesoscale convective system produced extreme rainfall over southeastern South Korea: 7 July 2009, *Mon. Weather Rev.*, doi:10.1175/MWR-D-16-0131.1.
Kawamura, R., and T. Murakami (1998), Baiu near Japan and its relation to summer monsoons over Southeast Asia and the western north Pacific, *J. Meteor. Soc. Jpn*, *76*, 619–639.
Kuo, H. L. (1974), Further studies of the parameterization of the influence of cumulus convection on large-scale flow, *J. Atmos. Sci.*, *31*, 1232–1240.
Lau, K. M., G. J. Yang, and S. H. Shen (1988), Seasonal and intraseasonal climatology of summer monsoon rainfall over East Asia, *Mon. Weather Rev.*, *116*, 18–37.
Liu, H. B., J. Yang, D. L. Zhang, and B. Wang (2014), Roles of synoptic to quasi-biweekly disturbances in generating the summer 2003 heavy rainfall in East China, *Mon. Weather Rev.*, *142*, 886–904.
Luo, Y., and Y. Chen (2015), Investigation of the predictability and physical mechanisms of an extreme-rainfall-producing mesoscale convective system along the Meiyu front in East China: An ensemble approach, *J. Geophy. Res. Atmos.*, *120*, 10,593–10,618, doi:10.1002/2015JD023584.
Mao, J., and G. Wu (2006), Intraseasonal variations of the Yangtze rainfall and its related atmospheric circulation features during the 1991 summer, *Clim. Dyn.*, *27*, 815–830.
Mao, J., S. Zhang, and G. Wu (2010), 20–50-day oscillation of summer Yangtze rainfall in response to intraseasonal variations in the subtropical high over the western North Pacific and South China Sea, *Clim. Dyn.*, *34*, 747–761.
Markowski, P., and Y. Richardson (2010), *Mesoscale Meteorology in Midlatitudes*, 407 pp., Wiley-Blackwell, Hoboken, N. J.
Murakami, S. (2011), Atmospheric local energetics and energy interactions between mean and eddy fields. Part I: Theory, *J. Atmos. Sci.*, *68*, 760–768.
Murakami, S., R. Ohgaito, and A. Abe–Ouchi (2011), Atmospheric local energetics and energy interactions between mean and eddy fields. Part II: An example for Last Glacial Maximum climate, *J. Atmos. Sci.*, *68*, 533–552.
Nagata, M., and Y. Ogura (1991), A modeling case study of interaction between heavy precipitation and a low-level jet over Japan in the baiu season, *Mon. Weather Rev.*, *119*, 1309–1336.
Ninomiya, K. (2000), Large–and meso-α-scale characteristics of meiyu/baiu front associated with intense rainfalls in 1–10 July 1991, *J. Meteor. Soc. Jpn.*, *78*, 141–157.
Oh, J. H., W. T. Kwon, and S. B. Ryoo (1997), Review of the researches on Changma and future observational study (KORMEX), *Adv. Atmos. Sci.*, *14*, 207–222.
Saha, S., et al. (2010), The NCEP climate forecast system reanalysis, *Bull. Am. Meteorol. Soc.*, *91*, 1015–1057, doi:10.1175/2010BAMS3001.1.
Sampe, T., and S. P. Xie (2010), Large-scale dynamics of the Meiyu–Baiu rainband: Environmental forcing by the westerly jet, *J. Clim.*, *23*, 113–134.
Sun, J. H., and T. Y. Lee (2002), A numerical study of an intense quasi-stationary convection band over Korean Peninsula, *J. Meteorol. Soc. Jpn.*, *80*, 1221–1245.
Sun, J. H., S. X. Zhao, G. K. Xu, and Q. T. Meng (2010), Study on a mesoscale convective vortex causing heavy rainfall during the mei-yu season in 2003, *Adv. Atmos. Sci.*, *27*, 1193–1209.
Tao, S. Y. (1980), *Rainstorms in China*, 225 pp., Sci. Press, Beijing.

Wang, C. C., C. Y. Kung, C. S. Lee, and G. T. J. Chen (2012), Development and evaluation of mei-yu season quantitative precipitation forecasts in Taiwan River Basins based on a conceptual climatology model, *Weather Forecasting*, *27*, 586–607.

Yang, H., and C. Li (2003), The relation between atmospheric intraseasonal oscillation and summer severe flood and drought in the Changjiang–Huaihe River basin, *Adv. Atmos. Sci.*, *20*, 540–553.

Yeh, H. C., G. T. J. Chen, and W. T. Liu (2002), Kinematic characteristics of a Mei-yu front detected by the QuikSCAT oceanic winds, *Mon. Weather Rev.*, *130*, 700–711.

Zhao, S. X., Z. Y. Tao, J. H. Sun, and N. F. Bei (2004), *Study on Mechanism of Formation and Development of Heavy Rainfalls on Meiyu Front in Yangtze River*, 282 pp., China Meteorol. Press, Beijing.